Conformational polymorphs of an oxalamide

Structural, Hirshfeld surface and theoretical analysis of two conformational polymorphs of *N,N'*-bis(pyridin-3-ylmethyl)oxalamide

Mukesh M. Jotani[*I], Julio Zukerman-Schpector,[*II] Lucas Sousa Madureira,[II] Pavel Poplaukhin,[III] Hadi D. Arman[IV], Tyler Miller[IV] and Edward R. T. Tiekink[*V]

[I] Department of Physics, Bhavan's Sheth R. A. College of Science, Ahmedabad, Gujarat 380001, India

[II] Laboratório de Cristalografia, Estereodinâmica e Modelagem Molecular, Departamento de Química, Universidade Federal de São Carlos, C.P. 676, São Carlos, SP, 13565-905, Brazil

[III] Chemical Abstracts Service, 2540 Olentangy River Rd, Columbus, Ohio, 43202, USA

[IV] Department of Chemistry, The University of Texas at San Antonio, One UTSA Circle, San Antonio, Texas 78249-0698, USA

[V] Research Centre for Crystalline Materials, Faculty of Science and Technology, Sunway University, 47500 Bandar Sunway, Selangor Darul Ehsan, Malaysia

Abstract. The common feature of two conformational polymorphs of *N,N'*-bis(pyridin-3-ylmethyl)oxalamide is their crystallisation in the monoclinic space group $P2_1/c$ with $Z = 4$. In low symmetry form **1**, the central core is effectively planar and the terminal pyridyl rings adopt a syn-periplanar conformation. In the high symmetry form, **2**, there are two independent molecules in the asymmetric unit but each is located about a centre of inversion. The rings again are almost perpendicular to the central plane but, from symmetry are anti-periplanar. Computational chemistry shows that symmetric molecules with syn (2-fold) and anti (centrosymmetric) conformations have nearly identical energies. In the molecular packing of each of **1** and **2**, supramolecular tapes based on amide-N–H…O(amide) hydrogen bonding are found. In **1**, these are connected into layers by C–H…N(pyridyl) interactions, while in **2**, the chains are linked into a three-dimensional architecture by C–H…N(pyridyl) interactions. The importance of hydrogen bonding is emphasised in the analysis of the Hirshfeld surfaces.

[*] Correspondence authors: mmjotani@rediffmail.com (M.M.J.); julio@power.ufscar.br (J.Z.-S.); edwardt@sunway.edu.my (E.R.T.T.)

Author	Title	File Name	Date	Page
Mukesh M. Jotani, Julio Zukerman-Schpector, Lucas Sousa Madureira, Pavel Poplaukhin, Hadi D. Arman, Tyler Miller and Edward R. T. Tiekink	Structural, Hirshfeld surface and theoretical analysis of two conformational polymorphs of *N,N'*-bis(pyridin-3-ylmethyl)oxalamide	3c_J_4.docx	30.10.2017	1 (22)

Introduction

Having both amide and pyridyl functionalities, the title compound, *N,N'*-bis(pyridin-3-ylmethyl)oxalamide (systematic name: *N,N'*-bis(pyridin-3-ylmethyl)ethanediamide, hereafter referred to as the diamide), see Figure 1, has attracted the attention of coordination chemists over the years. In this context, zero-dimensional [1], oligomeric [2] and coordination polymers [3-5] have been observed, including an intriguing case of a pair of interwoven coordination strands sustained by hydrogen bonding in tautomeric forms of the diamide [6]. In the realm of crystal engineering, several studies have appeared reporting co-crystal formation with carboxylic acids [7, 8] and, notably, the diamide featured in early studies investigating halogen bonding [9]. Despite this interest, the crystal structure of the parent diamide has yet to be described according to a search of the Cambridge Crystallographic Database [10]. In the course of studies of on-going investigations of the diamide and the isomeric species with 2- and 4-pyridyl substituents [11-14], we isolated crystals of the diamide from ethanol solution, this is labelled form **1** herein. Subsequently, a polymorphic form, **2**, was isolated from a failed co-crystallisation experiment in ethanol/chloroform (1/1 v/v) solution between the diamide and 2-(4-hydroxyphenylazo)benzoic acid, which has been employed recently in co-crystallisation experiments, with some measure of success, including with a related diamide [15-17]. Remarkably, two quite distinct conformations of the diamide were observed in the polymorphs and hence, are described as conformational polymorphs [18]. Herein, the results of a crystallographic and theoretical investigation of polymorphs **1** and **2** are described.
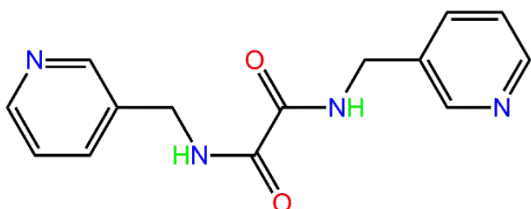

Fig. 1: Chemical structure of *N,N'*-bis(pyridin-3-ylmethyl)oxalamide, for which two monoclinic polymorphs have been characterised.

The discovery and study of polymorphs **1** and **2** is far beyond an intellectual curiosity. While the diamide shown in Figure 1 has yet proven any biological activity, the phenomenon of polymorphism is a crucial issue for the pharmaceutical industry [19] and also for energetic materials and dyes/pigments. Solid forms of drugs are patented as individual materials meaning the subsequent characterisation of a new form of a drug raises intellectual property (IP) issues. Based on the assumption that there is some tangible improvement in performance, if the pharmaceutical company that developed one form of a drug, subsequently discovers another form, patent extension of the pharmaceutical becomes a reality. An example of this is found in the saga associated with the histamine H2 inhibitor, ranitidine hydrochloride, used for the treatment of peptic ulcers. A new

Experimental

Synthesis and characterisation

N,*N*'-Bis(pyridin-3-ylmethyl)oxalamide was prepared in accord with the reported procedure [3]. Recrystallisation from ethanol solution, as in the original synthesis, gave **1**. Crystals of **2** were isolated from the attempted co-crystallisation of the diamide with 2-(4-hydroxyphenylazo)benzoic acid, 1:1 ratio, in an ethanol/chloroform mixture (1/1 v/v) solution.

Crystal structure determination

Intensity data for crystals of colourless **1** and **2** were collected at 98 K on a Rigaku AFC12/Saturn724 CCD fitted with Mo Kα radiation. The data set for **2** was corrected for absorption based on multiple scans [22] but not for **1** as no difference was manifested in the transmission factors. Each data set was reduced using standard methods [23]. Both structures were solved by direct methods [24] and refined by a full-matrix least-squares procedure on F^2 with anisotropic displacement parameters for non-hydrogen atoms, carbon-bound hydrogen atoms in their calculated positions, and a weighting scheme of the form $w = 1/[\sigma^2(F_o^2) + (aP)^2 + bP]$ where $P = (F_o^2 + 2F_c^2)/3$ [25]. The nitrogen-bound hydrogen atoms were refined with the distance restraint N–H = 0.88±0.01 Å. The analysis of **1** is less than optimal, e.g. high R_w, owing to the nature of the crystals obtained, an observation consistent with the fact that despite being originally synthesised over 20 years ago [3] and studied subsequently, see Introduction, no structure has been reported. Nevertheless, the molecular conformation has been determined unambiguously. Crystal data and refinement details are given in Table 1. Figure 1, showing the atom labelling schemes, was drawn with 50% displacement ellipsoids using ORTEP-3 for Windows [26], the overlay diagram was drawn with QMol [27], and the remaining crystallographic figures were drawn with DIAMOND [28]. Data interpretation was facilitated using PLATON [29].

Tab. 1: Crystallographic data and refinement details for **1** and **2**.[1]

Polymorph	1	2
Formula	$C_{14}H_{14}N_4O_2$	$C_{14}H_{14}N_4O_2$
Formula weight	270.29	270.29
Crystal colour, habit	block, colourless	prism, colourless
Crystal size/mm	0.20 x 0.20 x 0.20	0.10 x 0.14 x 0.40
Crystal system	monoclinic	monoclinic
Space group	$P2_1/c$	$P2_1/c$
a/Å	10.715(5)	10.106(2)
b/Å	5.096(2)	8.3088(16)
c/Å	23.846(12)	15.808(3)
β/°	97.342(7)	95.977(4)
V/Å^3	1291.3(10)	1320.2(4)
Z	4	4
D_c/g cm^{-3}	1.390	1.360
$F(000)$	568	568
$\mu(MoK\alpha)$/mm^{-1}	0.097	0.095
Measured data	4787	10286
θ range/°	2.4 – 25.0	2.6 – 27.5
Unique data	2230	3023
R_{int}	0.043	0.030
Observed data ($I \geq 2.0\sigma(I)$)	1849	2749
R, obs. data; all data	0.078; 0.088	0.040; 0.043
a; b in wghting scheme	0.177, 0.036	0.045, 0.629
R_w, obs. data; all data	0.238; 0.252	0.103; 0.106
Largest difference peak and hole (Å^{-3})	0.48, -0.54	0.41, -0.19

Hirshfeld surface analysis

Crystal Explorer 3.1 [30] was used to generate Hirshfeld surfaces mapped over $d_{norm,}$, d_e, curvedness and electrostatic potential. The electrostatic potentials were calculated using TONTO [31, 32] integrated into *Crystal Explorer*, wherein the experimental geometries were used as the input. Further, the electrostatic potentials were mapped on Hirshfeld surfaces using the STO-3G basis set at the Hartree-Fock level theory over a range of ±0.09 au. The contact distances d_i and d_e from the Hirshfeld surface to the nearest atom inside and outside, respectively, enable the analysis of the intermolecular interactions through the mapping of d_{norm}. The combination of d_e and d_i in the form of two-dimensional fingerprint plots [33] provides a useful summary of intermolecular contacts in the crystal.

Computational chemistry

The calculations were performed with the Firefly PC package [34], which is partially based on the GAMESS (US) [35] source code, at the B3LYP/6-31G** level of theory [36-39] with an algorithm based on the Quadratic Approximation (QA) [40] and a threshold gradient value of 10^{-5} a.u. Molecular parameters (bond order and partial charge) were evaluated by different models (Wiberg bond index and Giambiagi-Mayer bond orders, and Natural and Löwdin population analysis) [41-48].

Results and discussion

Experimental molecular structures

The molecular structure of **1** is shown in Figure 2a and features a central $C_4N_2O_2$ core, that, including the methylene-C6 and -C9 atoms, is planar with a r.m.s. deviation of the fitted atoms = 0.033 Å; the maximum deviation is 0.046(2) Å for the N2 atom. The N1- and N4-pyridyl rings are approximately normal to this plane and are synperiplanar, forming dihedral angles of 84.37(9) and 74.98(9)°, respectively with the central plane. The dihedral angle between the rings is 88.44(9)°, indicating an almost perpendicular relationship as each ring is directed away from the central part of the molecule. Selected geometric parameters are collated in Table 2. These reveal that the canonical form shown in Figure 1 is an accurate description of the electronic structure. The angles about the quaternary-C atom follow the expected trends with the widest angle involving the heteroatoms. The carbonyl-O atoms are anti, an arrangement that allows for the formation of intramolecular amide-N–H⋯O(carbonyl) hydrogen bonds, Table 3.
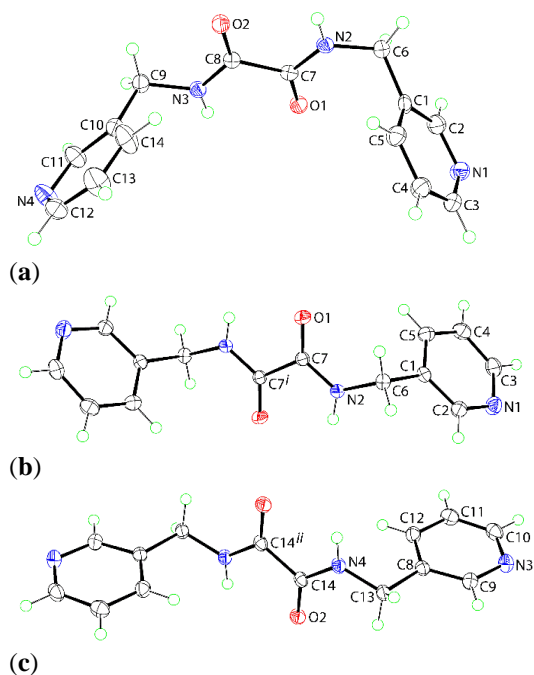

(a)

(b)

(c)

Fig. 2: Molecular structures of (**a**) **1**, (**b**) first independent molecule of **2**, and (**c**) second independent molecule of **2**. Each of the molecules in (**b**) and (**c**) are disposed about a centre of inversion with unlabelled atoms related by symmetry operations *i*: 1-*x*, 1-*y*, -*z* and *ii* -*x*, 2-*y*, 1-*z*, respectively. Displacement ellipsoids are drawn at the 50% probability level.

Tab. 2: Selected geometric parameters (Å, °) for **1** and **2**.[1]

1	value	2	value
C7–O1	1.235(3)	C7–O1	1.2303(14)
C8–O2	1.236(3)	C14–O2	1.2362(14)
N2–C7	1.327(4)	N2–C7	1.3266(15)
N3–C8	1.329(4)	N4–C14	1.3258(15)
N2–C6	1.459(3)	N2–C6	1.4655(15)
N3–C9	1.473(4)	N4–C13	1.4507(15)
C7–C8	1.544(4)	C7–C7^i	1.546(2)
		C14–C14^{ii}	1.538(2)
O1–C7–N2	125.5(3),	O1–C7–N2	125.70(11)
O2–C8–N3	125.7(3)	O2–C14–N4	125.98(11)
O1–C7–C8	121.7(2)	O1–C7–C7^i	120.84(13)
O2–C8–C7	121.2(2)	O2–C14–C14^{ii}	121.33(13)
N2–C7–C8	112.8(2)	N2–C7–C7^i	113.46(12)
N3–C8–C7	113.1(2)	N4–C14–C14^{ii}	112.68(12)

[1] Symmetry operations *i*: 1-*x*, 1-*y*, -*z* and *ii*: -*x*, 2-*y*, 1-*z*.

Tab. 3: Summary of intermolecular interactions (A–H···B; Å, °) operating in the crystal structures of **1** and **2**.

A	H	B	A–H	H···B	A···B	A–H···B	Symmetry operation
(**1**)							
N2	H2n	O2	0.878(19)	2.39(3)	2.706(3)	101.5(19)	*x, y, z*
N3	H3n	O1	0.880(18)	2.40(3)	2.719(3)	102.1(18)	*x, y, z*
N2	H2n	O1	0.878(19)	2.038(16)	2.860(4)	155(3)	*x*, -1+*y, z*
N3	H3n	O2	0.880(18)	2.029(15)	2.850(4)	155(3)	*x*, 1+*y, z*
C3	H3	N4	0.95	2.52	3.437(5)	163	*x*, 2½-*y*, ½+*z*
(**2**)							
N2	H2n	O1	0.874(11)	2.328(15)	2.7096(15)	106.6(10)	1-*x*, 1-*y*,-*z*
N4	H4n	O2	0.877(12)	2.299(14)	2.6975(15)	107.6(9)	-*x*, 2-*y*, 1-*z*
N2	H2n	O2	0.874(11)	2.054(10)	2.8563(14)	152.1(13)	-*x*, -½+*y*, ½-*z*
N4	H4n	O1	0.877(12)	2.003(10)	2.7898(14)	148.6(13)	1-*x*, ½+*y*, ½-*z*
C2	H2	N3	0.95	2.54	3.4333(18)	156	*x, y, z*
C13	H13A	N1	0.99	2.62	3.5935(18)	167	*x*, 1+*y, z*
C13	H13B	N3	0.99	2.51	3.3732(18)	146	-*x*, ½+*y*, ½-*z*

In polymorph **2**, two half independent molecules comprise the asymmetric unit as each is disposed about a centre of inversion, Figures 1b and c. The central eight atoms in each molecule have a r.m.s. deviation of 0.010 and 0.024 Å, from the respective least-squares plane, and the intramolecular amide-N–H…O(amide) hydrogen bonds persist, Table 3. The key difference between **1** and **2** relates to the relative disposition of the pyridyl rings which are anti-periplanar in **2**, that is, anti, forming similar dihedral angles of 76.21(4) and 77.08(4)°, respectively. The geometric parameters, Table 2, follow the same trends established for **1**.

Molecular packing

Parameters characterising the supramolecular aggregation in each of **1** and **2** are summarised in Table 3; prominent contacts have been taken from the PLATON [29] output based on the geometric criteria embodied in the program. The most prominent feature of the crystal packing in **1** is the formation of supramolecular tapes aligned along the b-axis and sustained by N–H…O hydrogen bonding between translationally related amide groups with the result that 10-membered $\{\cdots HNCCO\}_2$ synthons are formed, Figure 3a. Links between tapes along the c-axis are of the type pyridyl-C–H…N(pyridyl) to form corrugated layers in the bc-plane, Figure 3b. The layers interdigitate along the a-axis with no specific interactions between them, Figure 3c. The closest contact between pyridyl rings is 4.398(3) Å for symmetry operation x, $1\frac{1}{2}$-y, $\frac{1}{2}$+z. Within layers sustained by hydrogen bonding, some evidence was found for π-type interactions between the C_2O_2 cores as discussed below in the Hirshfeld surface analysis for **1**.
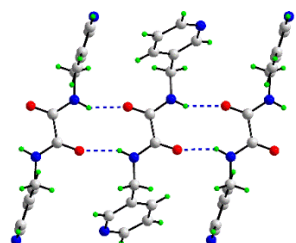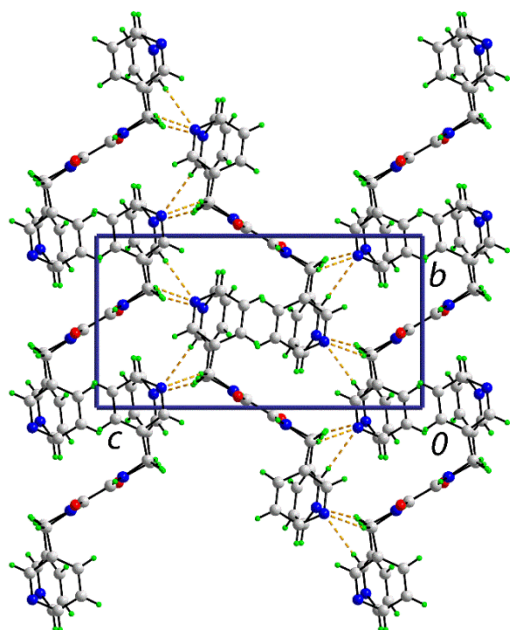

(a)

(b)
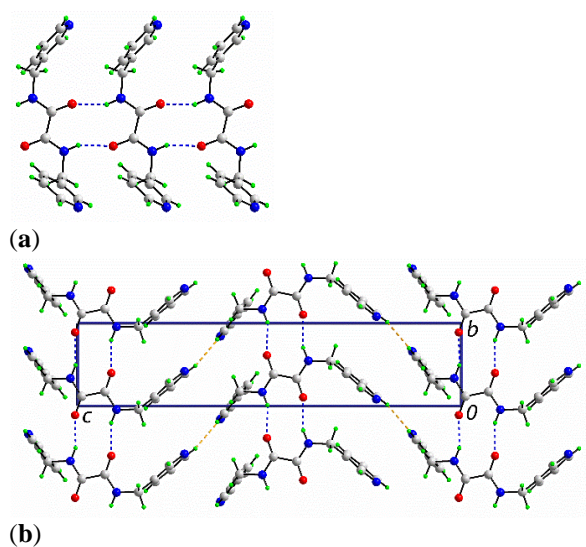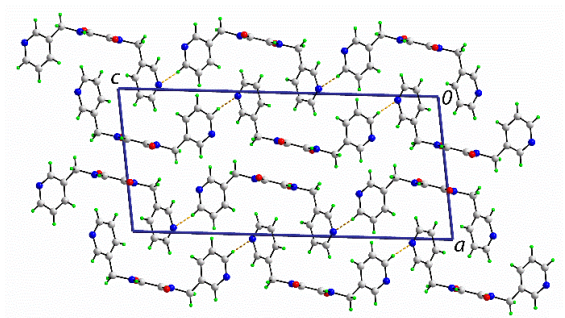
(c)

Fig. 3: Molecular packing in **1**: (**a**) A view of the supramolecular tape sustained by amide-N–H··O(amide) hydrogen bonds, (**b**) corrugated layers in the *bc*-plane whereby the tapes of (a) are linked by pyridyl-C–H··N(pyridyl) interactions, and (**c**) a view in projection down the *b*-axis highlighting the stacking of layers. The N–H··O and C–H··N interactions are shown as blue and orange dashed lines, respectively.

A very similar supramolecular tape is found in the crystal structure of **2**. Here, the tapes are aligned along the *a*-axis and comprise alternating independent molecules, Figure 4a. Unlike the situation in **1** where the pyridyl rings are superimposed when viewed down the axis of the tape, Figure 3a, in **2**, the pyridyl rings in successive molecules comprising the tape have different orientations. Globally, molecules assemble in the *ab*-plane with no specific interactions between but are connected to adjacent layers by methylene- and pyridyl-C–H··N(pyridyl) interactions so that a three-dimensional architecture results, Figure 4b.


(a)

(b)

Fig. 4: Molecular packing in **2**: (**a**) A view of the supramolecular tape sustained by amide-N–H···O(amide) hydrogen bonds, and (**b**) a view in projection down the *a*-axis highlighting the stacking of layers. The N–H···O and C–H···N interactions are shown as blue and orange dashed lines, respectively.

Hirshfeld surfaces

In order to gain a deeper appreciation of the supramolecular association in the polymorphs **1** and **2**, an analysis of the Hirshfeld surfaces was conducted [49]. The variation in the crystal packing interactions due to the different dispositions of the terminal pyridyl rings around the eight-membered oxalamide chromophore in polymorphs **1** and **2** can be conveniently discerned from the views of Hirshfeld surfaces. The molecular packing of both the polymorphs have similar intra- and inter-molecular N–H···O hydrogen bonds and intermolecular C–H···N bonds. The intermolecular interactions are evident from the views of Hirshfeld surfaces mapped over electrostatic potential, Figure 5. The donors and acceptor atoms participating in these interactions are shown with respective positive (blue regions) and negative potentials (red regions). In the plots mapped over d_{norm}, Figure 6, the bright-red spots on the surface indicate the atoms involved in the interactions.
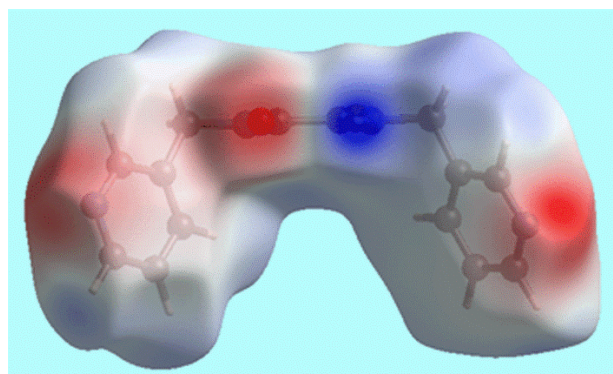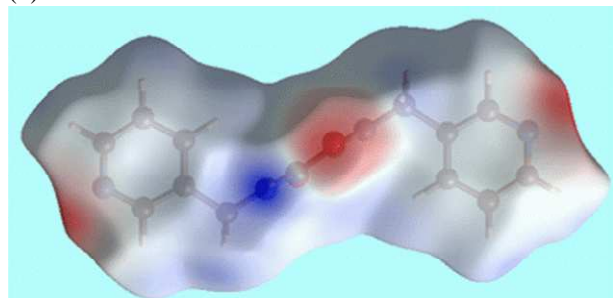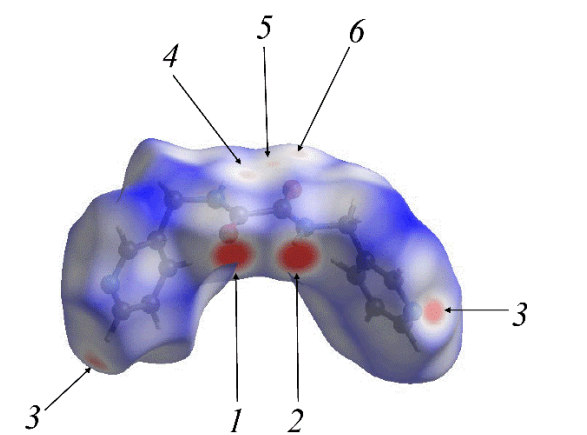
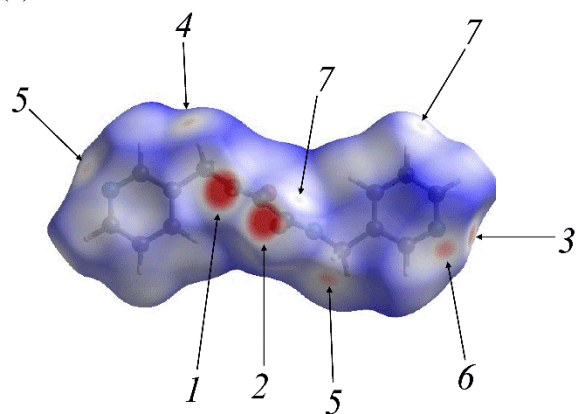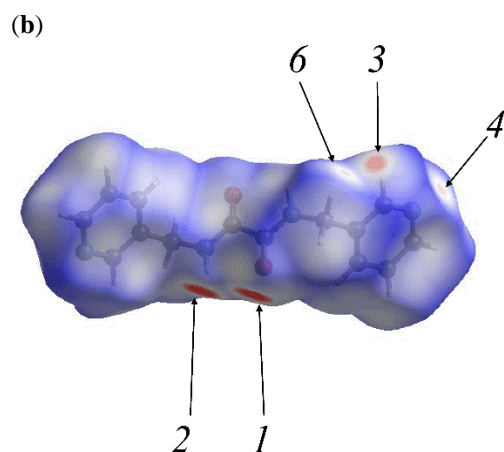**Fig. 5:** The electrostatic potential mapped over the Hirshfeld surfaces for (**a**) **1** and (**b**) **2**, second molecule, highlighting the regions of high electron density (red) and electropositive regions (blue).

(b)

(c)

Fig. 6: Views of d$_{norm}$ mapped over on the Hirshfeld surfaces, highlighting the regions involved in intermolecular N–H···O and C–H···N interactions: **(a) 1**, **(b) 2**, molecule 1, and **(c) 2**, molecule 2.

The common features of the molecular packing in **1** and **2**, are the intermolecular N–H···O and C–H···N interactions indicated as 1, 2 and 3 in Figures 6a-c. In the structure of **1**, the small but significant contributions from C···C and C···O/O···C contacts, Table 4, are due to the presence of short interatomic C8···C8 (3.330(4) Å) and C7···O2/O2···C7 (3.132(3) Å) distances and appear as pale-red spots on the Hirshfeld surfaces marked with the labels 4, 5 and 6 in Figure 6a; symmetry operation 1-x, 1-y, 1-z. The molecular packing of in **2** also features methylene-C–H···N and C–H···π interactions, and short interatomic non-bonded H···O and H···N contacts, highlighted as diminutive red spots and labelled as 4, 5, 6 and 7 in Figures 6b and c. The presence of these interactions may cause a slight increase in relative contributions from N···H/H···N contacts to the surface of both molecules of **2**, and of O···H/H···O to the surface of the second molecule of **2** compared to that in **1**, Table 4. The appearance of a pale-orange spot on the surface mapped over d$_e$, within a red circle in Figure 7a, and a bright-red spot over the front side of shape-index, Figure 7b, reflect the contribution of the C–H···π interactions. The reciprocal of these C–H···π interactions, i.e. π···H–C, is seen as a blue spot on the surface mapped with the shape index, Figure 7b.

Tab. 4: Percentage contributions of various intermolecular contacts to the Hirshfeld surface areas of **1** and **2**, the latter delineated for the two independent molecules.

Contact	% contribution		
	1	**2**	
		First molecule	Second molecule
H···H	44.1	35.8	36.9
O···H/H···O	15.7	14.2	19.6
N···H/H···N	16.7	18.0	19.5
C···H/H···C	16.7	31.4	22.4
C···C	2.7	0.1	0.3
C···O/O···C	2.1	0.1	0.1
C···N/N···C	1.8	0.4	1.1

| Others | 0.2 | 0.0 | 0.1 |
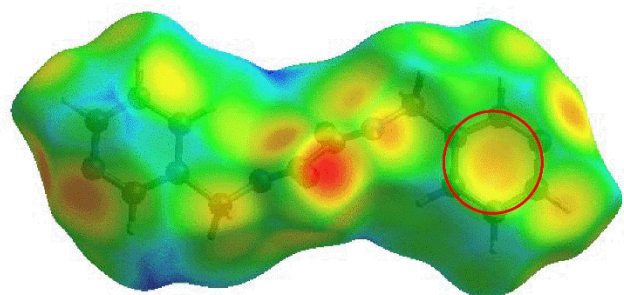
(a)
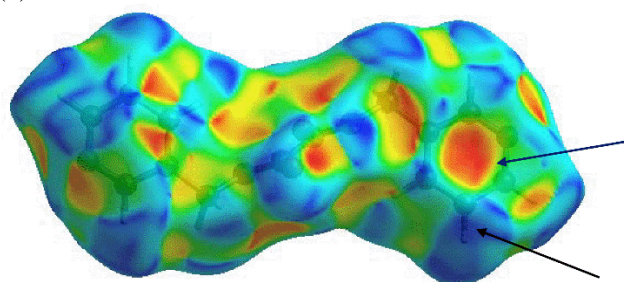
(b)

Fig. 7: Hirshfeld surface mapped for **2**, molecule 1: (a) over d_e, and (b) with shape-index, with arrows indicating the presence of C···H/H···C contacts

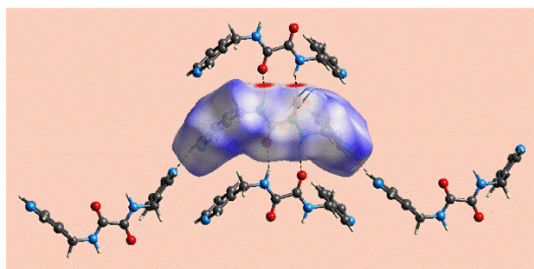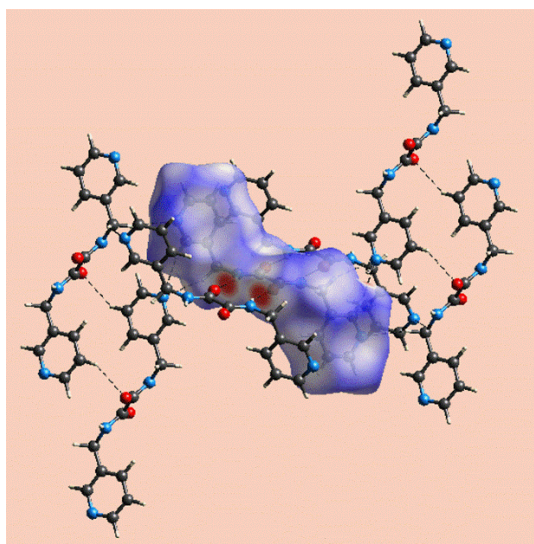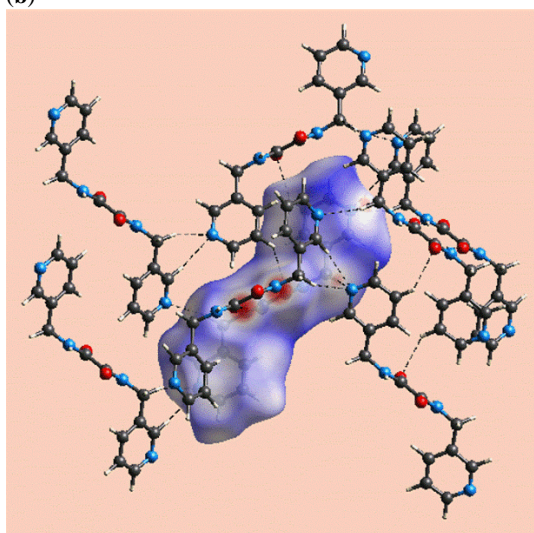Figure 8 presents images of the immediate environment about the different molecules in **1** and **2**, and provides a convenient visual summary of the interactions between molecules.

(a)

(b)

(c)

Fig. 8: Views of the Hirshfeld surfaces mapped over d_{norm} emphasising the interaction environment about a reference molecule in (**a**) **1**, (**b**) **2**, molecule 1, and (**c**) **2**, molecule 2.

The two-dimensional fingerprint (FP) plots, Figure 9, explain the formation of the distinct three-dimensional arrangements in **1** and **2** through the various interactions involving the different molecules. The overall FP plots for **1** and **2** (molecules 1 and 2), Figure 9a, show that the points are distributed distinctly, and in this way provide further evidence of the choice of the space group for **2**, with two independent, centrosymmetric molecules.

The FP plots delineated into H···H contacts for **2**, Figure 9b, have two small adjacent peaks at $d_e = d_i \sim 1.2$ Å, and the green points in the central region show greater density; the points scattered in broader area of plots with the single peak at the same d, d_i distance is common for both molecules. The similar characteristic pairs of spikes at $d_e + d_i \sim 1.9$ Å appearing in the plots of all three molecules confirms the formation of almost identical intermolecular N–H···O hy-

drogen bonds involving the same atoms of the oxalamide chromophores, Figure 9c. The FP plots delineated into N···H/H···N contacts for both molecules of **2** show similar spear-like pairs with tips at $d_e + d_i \sim 2.4$ Å and indicate almost similar conformations, Figure 9d. The "forceps" in the FP plot of **1** arises as a result of the syn orientation of terminal pyridyl rings, Figure 9d. Figure 9e shows the FP plots delineated into the C···H/H···C contacts, which exhibit different shapes for **1** and **2**, and have quite disparate relative contributions, Table 4. A common feature of these plots is the appearance of a pair of characteristic 'wings' and a pair of arrow-like shapes extending over the (d_e, d_i) regions between 1.1 and 2.6 Å.

The intermolecular interactions were further analysed using a new parameter, namely the enrichment ratio (ER) which is evaluated on the basis of Hirshfeld surface analysis [50]; the numerical values are listed in Table 5. The ER value corresponding to H···H contacts is close to unity for **1** in accord with earlier published data [50]. By contrast, the corresponding values for molecules 1 and 2 of **2** are reduced to 0.78 and 0.81, respectively, showing a lower propensity for these contacts in the crystal structure. This may be due to the involvement of hydrogen atoms in intermolecular methylene-C–H···N and C–H···π interactions in **2** which in turn increase the ER values corresponding to C···H/H···C contacts. The lower ER value for the latter contacts in **1** correlates with the absence of comparable interactions in its structure.

The occurrence of short inter atomic C···C and C···O/O···C contacts in the structure of **1** are also evident from their respective ER values and prove the importance of their relatively small contributions to the Hirshfeld surface due to the lower random contacts resulting from 13.0 and 9.0% available surfaces for carbon and oxygen atoms, respectively. Molecules 1 and 2 of **2** have negligible contributions from the contacts correlating to their absence.

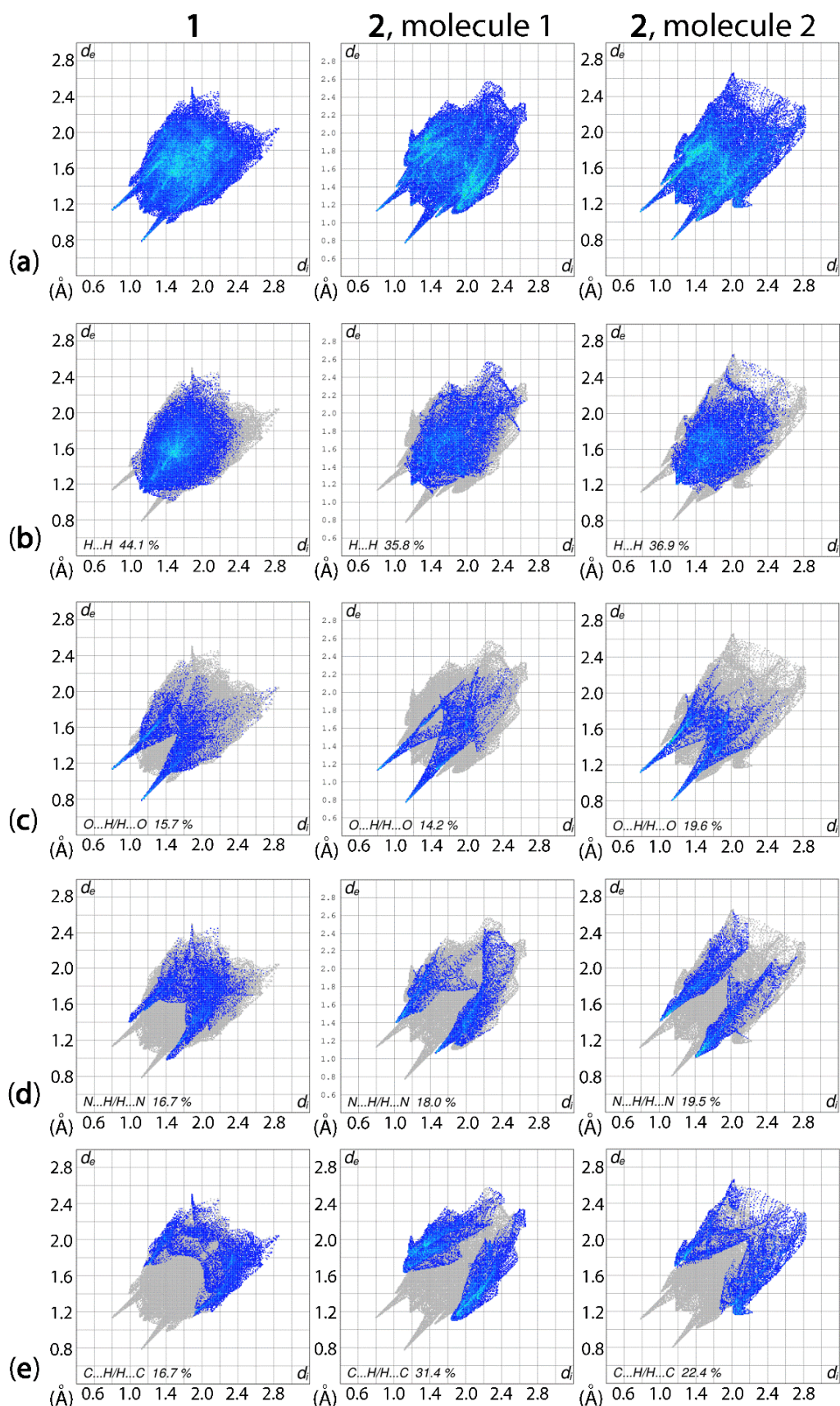**Fig. 10:** Fingerprint plots calculated for **1** and **2** (delineated into the two independent molecules): (**a**) overall plot, and plots delineated into (**b**) H···H, (**c**) O···H/H···O, (**d**) N···H/H···N and (**e**) C···H/H···C contacts.

Tab. 5: Enrichment ratios for of **1** and **2**, the latter delineated for the two independent molecules.

Contact	**1**	**2**	
		First molecule	Second molecule
H⋯H	0.94	0.78	0.81
O⋯H/H⋯O	1.28	1.47	1.47
N⋯H/H⋯N	1.31	1.45	1.40
C⋯H/H⋯C	0.94	1.45	1.37
C⋯C	1.60	–	–
C⋯O/O⋯C	0.90	–	–

Computational Chemistry

Recently, a full theoretical analysis of the conformational preferences of the isomeric *N,N'*-bis(pyridin-n-ylmethyl)thioxalamide derivatives, n = 2, 3 and 4, i.e. the thio derivatives related to **1** and **2**, was published [51]. Similar protocols were employed in the present investigation in order to gain insight into the great conformational differences exhibited in polymorphs **1** and **2**, as illustrated in the overlay diagram, Figure 10.
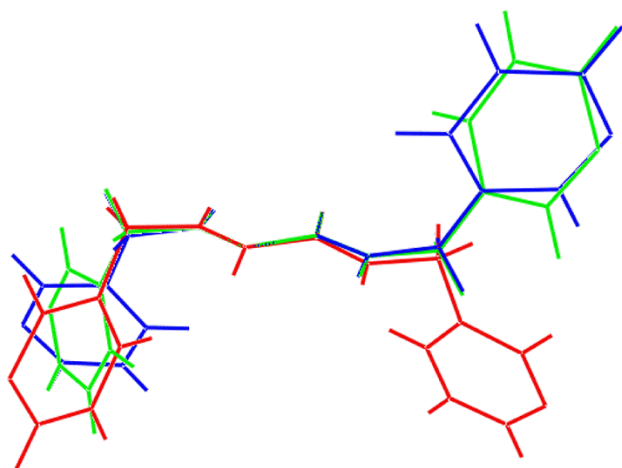
Fig. 10: Overlay diagram of the three experimental conformations found for the *N,N'*-bis(pyridin-3-ylmethyl)oxalamide molecule in polymorphs **1** (red image) and **2** – first independent molecule (green) and second molecule (blue).

The first question addressed related to the conformation about the N–C(=O) bonds, i.e. the global conformation in the central residue. Based on the assumption of multiple bond character in the N–C bond (see below), the different conformations can be labelled as ZZ, EZ and EE, see Figure 11 for images of the different conformations. From the data in Table 6, the all Z conformation is clearly the most stable. This observation correlates with the intramolecular N–H…O hydrogen bonds which close S(5) loops in the ZZ conformation, Table 3, only one of these persists in the EZ form and none in the all E arrangement. For the related thioamide compounds [51], the reduction in the N–H…S

hydrogen bonds results in a reduced energy of stabilisation to the overall conformation in the EZ and, especially, EE conformations. The new results are therefore consistent with the literature [51].
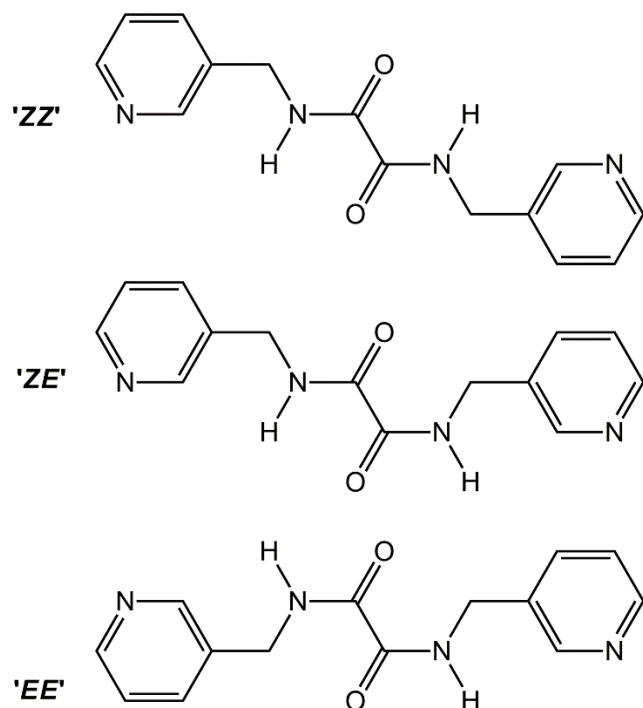

Fig. 11: Envisaged isomers for *N,N'*-bis(pyridin-3-ylmethyl)oxalamide. The Z/E designation refers to the relative positioning of the methylene-C and carbonyl-O atoms, on both sides of the molecule, which may be interchanged by rotation about the N–C(methylene) bond.

Tab. 6: Relative energies at 298.15 K and in kcal.mol^{-1} of possible conformers of *N,N'*-bis(pyridin-3-ylmethyl)oxalamide, as calculated from theory

Conformer	$\Delta G°$	ΔE_{ZPE}	ΔE
ZZ	0	0	0
ZE	6.1	5.9	6.0
EE	11.6	10.6	10.6

Having established the global stability of the ZZ conformation, attention was then directed toward establishing the relative stability of the different conformations of the pyridyl residues with respect to the central residue; these were generated by rotations about the methylene-C–C(pyridyl) bond. Four low-energy conformations, differing by no more than 1 kcal/mol were revealed, Table 7. Two conformations were based on the letter U, i.e. with the pyridyl ring syn with respect to the central plane. One option with lowest energy has C_2 symmetry with a non-symmetric form, as in **1**, being marginally higher in energy. The S-shaped option with inversion symmetry, as in **2**, had the same energy as the symmetric U-shape; the non-

symmetric S-shape was 0.4 kcal/mol higher in energy. These calculations suggest that polymorph **2** is the more stable, by 0.5 kcal/mol.

Tab. 7: Relative energies at 298.15 K and in kcal.mol^{-1} for four relative conformations of the pyridyl rings in *N,N'*-bis(pyridin-3-ylmethyl)oxalamide, as calculated from theory.

Conformer	$\Delta G°$	ΔE_{ZPE}	ΔE
U (2-fold)	0.0	0.0	0.0
U (non-symmetric)	0.5	0.7	0.7
S (centrosymmetric)	0.0	0.0	0.1
S (non-centrosymmetric)	0.4	0.5	0.7

One final point concerning the molecular structures is worth highlighting, namely, the magnitude of the central C-C bond. This is unusually long for a standard sp^2-C–C(sp^2) bond and usually attracts a level C alert in PLATON [29]. In the following discussion, the S-centrosymmetric molecule was chosen for analysis as this conformation is normally observed in co-crystals/salts formed by the diamide described herein [52]. In this energy-minimised structure, the central C–C bond length is 1.543 Å, and is in accord with the experimental values, Table 2. The bond order data collated in Table 8 is consistent with delocalisation of π-electron density over the oxygen and nitrogen atoms of the central residue which results in increasing π-character in the C–N bond with a concomitant reduction in the double bond character of the C=O bond, as discussed previously for the thioamide analogues [51].

Tab. 8: Calculated bond orders and charges (*e*) within the amide group in the energy minimised structure (S-centrosymmetric) of *N,N'*-bis(pyridin-3-ylmethyl)oxalamide.

Bond	C=O	C–N	C–C
Giambiagi-Mayer bond orders			
	1.683	1.158	0.883
Wilberg bond index			
	1.614	1.251	0.909
Atom	carbonyl-O	amide-N	central-C
NPA charges (*e*)			
	-0.642	-0.628	0.605
Löwdin charges (*e*)			
	-0.144	-0.321	0.128

Author	Title		File Name	Date	Page
Mukesh M. Jotani, Julio Zukerman-Schpector, Lucas Sousa Madureira, Pavel Poplaukhin, Hadi D. Arman, Tyler Miller and Edward R. T. Tiekink	Structural, Hirshfeld surface and theoretical analysis of two conformational polymorphs of *N,N'*-bis(pyridin-3-ylmethyl)oxalamide		3c_J_4.docx	30.10.2017	19 (22)

Conclusions

Two polymorphs have been characterised for *N,N'*-bis(pyridin-3-ylmethyl)oxalamide, a syn-periplanar (**1**) and an anti-periplanar form (**2**). These are examples of conformational polymorphism for which a recent survey suggested 74% of examples had energy differences less than 1.5 kcal/mol [53]. Computational chemistry suggests that the 2-fold symmetric syn form is equal in energy to the centrosymmetric anti form. While the non-symmetric syn form found experimentally is less stable, no doubt the loss in stability corresponding to the loss of symmetry is compensated by global crystal packing effects. Vindicating this conclusion are the crystal packing indices of 71.7 and 69.9%, respectively. Further, it is noted that syn and anti forms of a closely related molecule, 4-[2-(pyridin-4-yl)ethyl]pyridine, are found within the same crystal structure, i.e. in its 1:1 co-crystal with bis(2-hydroxyphenyl)-4-hydroxyphenylmethane [54]. Finally, it is noted that **2** was isolated from a failed co-crystallisation experiment. As noted by Arora and Zaworotko, co-crystallisation experiments often result in the isolation of a new polymorph of one of the coformers. It was also suggested such technology should be employed in any thorough polymorph screen of active pharmaceutical ingredients [55].

References

[1]   X. Li, X. He, Y. Chen, X. Fan, Q. Zeng, *J. Mol. Struct.* **2011**, *1002*, 145.

[2]   Z. Qin, M. C. Jennings, R. J. Puddephatt, *Inorg. Chem.* **2003**, *42*, 1956.

[3]   C. L. Schauer, E. Matwey, F. W. Fowler, J. W. Lauher, *J. Am. Chem. Soc.* **1997**, *119*, 10245.

[4]   D. L. Reger, D. M. C. Smith, K. D. Shimizu, M. D. Smith, *Polyhedron* **2004**, *23,* 711.

[5]   Q. Zeng, M. Li M, D. Wu, S. Lei, C. Liu, L. Piao, Y. Yang, S. An, C. Wang, *Cryst. Growth. Des.* **2008**, *8*, 869.

[6]   P. Poplaukhin, E.R.T Tiekink, *CrystEngComm* **2010**, *12*, 1302.

[7]   T. L. Nguyen, F. W. Fowler, J. W. Lauher, *J. Am. Chem. Soc.* **2001**, *123*, 11057.

[8]   H. D. Arman, T. Miller, P. Poplaukhin, E. R. T. Tiekink, *Acta Crystallogr. E* **2010**, *66*, o2590.

[9]   N. S. Goroff, S. M. Curtis, J. A. Webb, F. W. Fowler, J. W. Lauher, *Org. Lett.* **2005**, *7*, 1891.

[10] C. R. Groom, I. J. Bruno, M. P. Lightfoot, S. C. Ward, *Acta Crystallogr. B*, **2016**, *72*, 171.

[11] H. D. Arman, T. Miller, P. Poplaukhin, E. R. T. Tiekink, *Z. Kristallogr.* **2013**, *228*, 295.

[12] H. D. Arman, T. Miller, E. R. T. Tiekink, *Z. Kristallogr.* **2012**, *227*, 825.

[13] H. D. Arman, T. Kaulgud, T. Miller, P. Poplaukhin, E. R. T. Tiekink, *J. Chem. Crystallogr.* **2012**, *42*, 673.

[14] P. Poplaukhin, H. D. Arman, E. R. T. Tiekink, *Z. Kristallogr.* **2012**, *227*, 363.

[15] H. D. Arman, T. Miller, P. Poplaukhin, E. R. T. Tiekink, *Acta Crystallogr E* **2009**, *65*, o3178.

[16] H. D.Arman, T. Miller, E. R. T. Tiekink, *Acta Crystallogr E* **2009**, *65*, o3226

[17] E. M. Corlette, E. R. T. Tiekink, *J. Chem. Crystallogr.* **2009**, *39*, 603.

[18] A. J. Cruz-Cabeza, J. Bernstein, *Chem. Rev.* **2014**, *114*, 2170.

[19] R. Hilfiker (Ed.) in Polymorphism in the Pharmaceutical Industry, Wiley-VCH, Germany, 2006.

[20] S. L. Price, Chem. Soc. Rev. **2014**, *43*, 2098.

[21] J. Bernstein, Polymorphism in Molecular Crystals, Oxford Science Publications, Clarendon Press, Oxford, England, 2002.

[22] T. Higashi. ABSCOR. Rigaku Corporation, Tokyo, Japan, **1995**.

[23] CrystalClear-SM Expert. User Manual. Rigaku/MSC Inc., Rigaku Corporation, The Woodlands, TX, **2011**.

[24] G. M. Sheldrick, *Acta Crystallogr. A* **2008**, *64*, 112.

[25] G. M. Sheldrick, *Acta Crystallogr. C* **2015**, *71*, 3.

[26] L. J. Farrugia, *J. Appl. Crystallogr.* **2012**, *45*, 849.

[27] J. Gans, D. Shalloway, *J. Mol. Graph. Model.* **2001**, *19*, 557.

[28] DIAMOND, Visual Crystal Structure Information System, Version 3.1, CRYSTAL IMPACT, Postfach 1251, D-53002, **2006**.

[29] S. K. Wolff, D. J. Grimwood, J. J. McKinnon, M. J. Turner, D. Jayatilaka, M. A. Spackman, Crystal Explorer (Version 3.1), University of Western Australia, **2012**.

[30] M. A. Spackman, J. J. McKinnon, D. Jayatilaka, *CrystEngComm* **2008**, *10*, 377.

[32] D. Jayatilaka, D. J. Grimwood, A. Lee, A. Lemay, A. J. Russel, C. Taylor, S. K. Wolff, C. Chenai, A. Whitton, TONTO – A System for Computational Chemistry, **2005**. Available at: http://hirshfeldsurface.net/

[33] J. J. McKinnon, M. A. Spackman, A. S. Mitchell, *Acta Crystallogr. B* **2004**, *60*, 627.

[34] A. A. Granovsky, Firefly version 8.1.1; http://classic.chem.msu.su/gran/firefly/index.html

[35] M.W. Schmidt, K.K. Baldridge, J.A. Boatz, S.T. Elbert, M.S. Gordon, J.H. Jensen, S. Koseki, N. Matsunaga, K.A. Nguyen, S. Su, T.L. Windus, M. Dupuis, J.A. Montgomery, *J.Comput.Chem.* **1993**, *14*, 1347.

[36] A. D. Becke, *J. Chem. Phys.* **1993**, *98*, 5648.

[37] W. J. Hehre, R. Ditchfield, J. A. Pople, *J. Chem. Phys.* **1972**, *56*, 2257.

[38] M. M. Francl, W. J. Petro, W. J. Hehre, J. S. Binkley, M. S. Gordon, D. J. DeFrees, J. A. Pople, *J. Chem. Phys.* **1982**, *77*, 3654.

[39] P. C. Hariharan, J. A. Pople, *Theoret. Chim. Acta* **1973**, *28*, 213.

[40] F. Jensen, *J. Chem. Phys.* **1995**, *102*, 6706.

[41] NBO 5.G. E. D. Glendening, J. K. Badenhoop, A. E. Reed, J. E. Carpenter, J. A. Bohmann, C. M. Morales, F. Weinhold, (Theoretical Chemistry Institute, University of Wisconsin, Madison, WI, http://www.chem.wisc.edu/~nbo5

[42] A. E. Reed, P. V. R. Schleyer, *Inorg. Chem.* **1988**, *27*, 3969.

[43] K. B. Wiberg, *Tetrahedron* **1968**, *24*, 1083.

[44] A. J. Bridgeman, G. Cavigliasso, L. R. Ireland, J. Rothery, *J. Chem. Soc. Dalton Trans.* **2001**, 2095.

[45] I. Mayer, P. Salvador, *Chem. Phys. Lett.* **2004**, *383*, 368.

[46] A. E. Reed, R. B. Weinstock, F. Weinhold, *J. Chem. Phys.* **1985**, *83*, 735.

[47] P. O. Löwdin, *J. Chem. Phys.* **1950**, *18*, 365.

[48] G. Bruhn, E. T. R. Davidson, I. Mayer, A. E. Clark, *Int. J. Quant. Chem.* **2006**, *106*, 2065.

[49] J. J. McKinnon, A. S. Mitchell, M. A. Spackman, Chem. – A Eur. J. **1998**, *4*, 2136.

[50] C. Jelsch, K. Ejsmont, L. Huder, *IUCrJ* **2014**, *1*, 119.

[51] J. Zukerman-Schpector, L. Sousa Madureira, P. Poplaukhin, H. D. Arman, T. Miller, E. R. T. Tiekink, *Z. Kristallogr.* **2015**, *230*, 531.

[52] S. Syed, S. N. A. Halim, M. M. Jotani and E. R. T. Tiekink, *Acta Crystallogr. E* **2016**, *72*, 76.

[53] A. J. Cruz-Cabeza, S. M. Reutzel-Edens, J. Bernstein, *Chem. Soc. Rev.*, **2015**, *44*, 8619.

[54] A. Jayaraman, V. Balasubramaniam, S. Valiyaveettil, *Cryst. Growth Des.* **2006**, *6*, 150.

[55] K. K. Arora, M. J. Zaworotko, in H. G. Brittain (Ed.), Polymorphism in Pharmaceutical Solids. Vol. 2. Informa Healthcare, pp. 281, **2009**.